Journal of Materials Science: Materials in Electronics (2020) 31:8796–8804
https://doi.org/10.1007/s10854-020-03414-7

Ternary $TiO_2/MoSe_2$/γ-graphyne heterojunctions with enhanced photocatalytic hydrogen evolution

Lulu Wu[1] · Qiaodan Li[1] · Chaofan Yang[1] · Yang Chen[1] · Zhaoqing Dai[1] · Boyu Yao[1] · Xiaoyan Zhang[2] · Xiaoli Cui[1]

Received: 2 February 2020 / Accepted: 13 April 2020 / Published online: 22 April 2020

Abstract
Photocatalytic water splitting for hydrogen evolution is widely considered as a clean, green, and renewable route for solar energy conversion and storage. In this work, we fabricated ternary $TiO_2/MoSe_2$/γ-graphyne nanocomposite and demonstrated its superior photocatalytic hydrogen evolution activity. The samples were investigated by transmission electron microscopy, UV–Vis diffuse reflectance spectra, electrochemical impedance spectroscopy, and photoluminescence spectra. The optimized sample exhibited a high H_2 production rate of 16 μmol h^{-1}, which was 3.2-fold as high as that of binary $TiO_2/MoSe_2$ and 6.2-fold as high as that of pristine TiO_2. The enhanced photocatalytic activity is mainly because of the higher light-harvesting capacity, more active edge sites, and more charge-transfer channels induced by the multicomponent heterojunction through a cascade-driven electronic mechanism. This work presents a practical way to design noble-metal-free photocatalysts for solar energy-driven water splitting by band-engineering tailoring.

1 Introduction

In recent years, a huge surge of interest has developed in the field of solar energy utilization, particularly in the application of photocatalytic hydrogen evolution to tackle the problem of energy shortage and environmental pollution [1–3]. Semiconductors such as TiO_2 [4–6], ZnO [7], CdS [8], and C_3N_4 [9] have been reported to be active for photocatalytic hydrogen evolution. Among these, TiO_2 is a promising and benchmark photocatalyst because of its low-cost, high chemical stability, and environmentally friendly features. However, TiO_2 bears the inferior photocatalytic activities that are caused by its wide bandgap and high recombination rate of electron–hole pairs, which hinders its commercial application [5]. To get higher photocatalytic activities of TiO_2, massive efforts have been contributed through surface treatment [10], element doping [11], cocatalysts loading [12], and heterojunction-structure modification [13–15]. Ternary photocatalysts, i.e., photocatalysts modified with both holes cocatalysts and electrons cocatalysts, have the superiority of stronger built-in electric field and efficient channeling for charge transfer, compared with unary or binary photocatalysts [16–20]. Rational design and nanoscale integration of multiple functional nanoscale components are reported to lead improved photocatalytic activities and stability. For example, the proposal of both TiO_2/MoS_2/CdS tandem heterojunction photocatalyst [16] and TiO_2/MoS_2/graphene composite [17] consistently demonstrated the enhanced photocatalytic hydrogen evolution.

2D transition metal dichalcogenides (TMDs) including MoS_2, WS_2, and $MoSe_2$ have gradually become a hot point in the field of photocatalysis due to their speedy electron migration ability and superior light absorption performance [21–25]. Furthermore, large amounts of active sites for hydrogen generation around the crystal edges of TMDs could enhance the reaction efficiency of the proton reduction process [23, 24]. As one of the typical TMDs, $MoSe_2$ has a bandgap of 1.7–1.9 eV, showing a wide range of light absorption [26–30]. Besides, $MoSe_2$ has lower cost and more abundant reserves than other cocatalysts such as noble metal and graphene [31–34]. Previous works have proven that

Electronic supplementary material The online version of this article (https://doi.org/10.1007/s10854-020-03414-7) contains supplementary material, which is available to authorized users.

✉ Xiaoyan Zhang
xyzhang_dd@shu.edu.cn

✉ Xiaoli Cui
xiaolicui@fudan.edu.cn

[1] Department of Materials Science, Fudan University, Shanghai 200433, China

[2] Department of Chemistry, Shanghai University, Shanghai 200444, China

$MoSe_2$ nanosheets can accept electrons and act as active sites for H_2 evolution, which results in that the $MoSe_2/TiO_2$ nanocomposite has higher photocatalytic performance than pure TiO_2 [33]. However, the photocatalytic water splitting activity for hydrogen evolution based on semiconductor photocatalysts is still far away from the practical application, requiring a solar-to-hydrogen conversion efficiency of 10% [35]. Thus it is still a big challenge to further improve the photocatalytic performance of TiO_2.

Graphyne is a new family of two-dimensional (2D) nanostructured carbon materials with sp and sp^2-hybridized carbon atoms. The theoretical calculation shows that graphyne has abundant and adjustable electronic structures, unique semiconductor transport properties and uniformly dispersed channel structures[36–38]. Since its first synthesis in 2010 by Li et al., it has been experimentally demonstrated to be a promising material in energy and environmental fields [39–44]. For instance, graphdiyne (GDY) has been used as the hole transfer layer into a photoelectrochemical water splitting cell for hydrogen production [43]. Lu et al. combined graphdiyne with g-C_3N_4 to enhance the hole mobility in a metal-free 2D/2D g-C_3N_4/GDY heterojunction [44]. Different from γ-GDY, γ-graphyne can be seen as an acetylene bond inserted between the adjacent carbon hexagonal rings. Among all kinds of graphyne, γ-graphyne is theoretically reported to possess the highest stability and semiconductor characteristic, and thus attracts more attention in energy conversion and storage applications [45–49]. In our recent work, we reported a mechanochemistry route to synthesize γ-graphyne [47] and constructed TiO_2/γ-graphyne heterojunctions, which improved the absorption of visible light and suppressed the recombination of photoexcited electron–hole pairs during the photocatalytic process [48].

Based on our previous and preliminary research, the conductive band positions for $MoSe_2$, TiO_2 and γ-graphyne were found to be 5, − 0.3 and − 0.5 V *vs* NHE, respectively. Therefore, a higher photocatalytic activity is expected if γ-graphyne, $MoSe_2$ and TiO_2 are combined together, since $MoSe_2$ nanosheets can accept electrons and act as active sites for H_2 evolution and γ-graphyne could transfer holes efficiently. Herein, novel $TiO_2/MoSe_2$/γ-graphyne ternary nanocomposites were synthesized and its photocatalytic H_2 evolution performance was demonstrated. As expected, the optimized $TiO_2/MoSe_2$/GY sample exhibited a high H_2 production rate of 16 μmol h^{-1}, which was 3.2-fold as high as that of $TiO_2/MoSe_2$ and 6.2-fold as high as that of TiO_2. The enhanced photocatalytic activity of the ternary photocatalyst was due to its improved light absorption, the formed heterojunction, and the role of the $MoSe_2$ nanosheets as an electron acceptor. Scheme 1 exhibited the schematic illustration of the charge transfer in $TiO_2/MoSe_2$/GY nanocomposites. This study offers significant insights toward the rational design of noble-metal-free titania-based composites for highly efficient photocatalytic reactions.

2 Experimental section

2.1 *Preparation of $TiO_2/MoSe_2$ nanosheets heterojunctions*

$TiO_2/MoSe_2$ nanocomposite with an optimized loading of 0.1% $MoSe_2$ was fabricated by the one-step hydrothermal method reported in our previous work [33]. Typically, 100 mg commercial P25 powders and 60 mL of 2:1 ethanol/deionized water solution were firstly added to a 100 ml beaker. Then, 1 mL layered $MoSe_2$ dispersion that synthesized through a reported liquid-phase exfoliation method [34] was added into the mixture. After magnetically stirring for 2 h, the mixture was transferred into a 100 mL Teflon-lined autoclave, sealed, and heated in an oven at 120 °C for 3 h. The products were rinsed with deionized water and dried at 60 °C overnight. The obtained sample were expressed as $TiO_2/MoSe_2$.

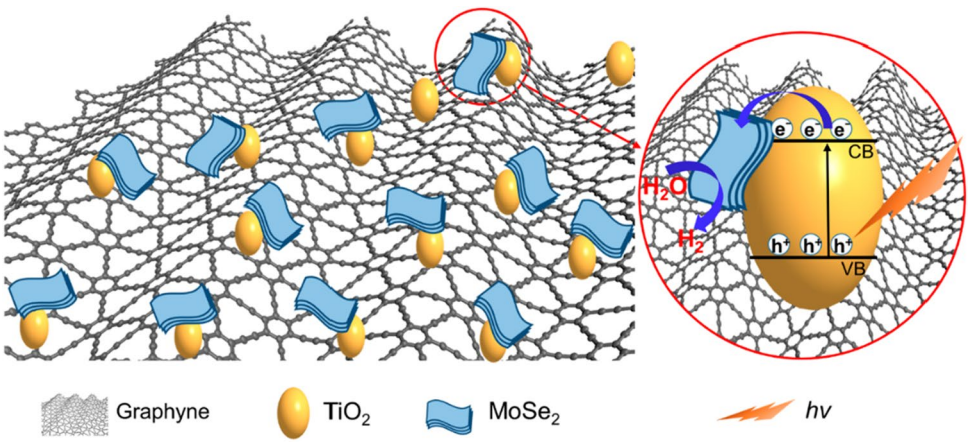

Scheme 1 Schematic illustration of the $TiO_2/MoSe_2$/GY nanocomposites for photocatalytic reactions

2.2 *Preparation of TiO_2/$MoSe_2$/γ-graphyne heterojunctions*

γ-Graphyne was synthesized using CaC_2 and hexabromobenzene ($PhBr_6$) as precursors through a mechanochemical route [47]. The TiO_2/$MoSe_2$/γ-graphyne heterojunctions were prepared as follows: 1 mg γ-graphyne, 40 mL absolute ethanol were dispersed in 20 mL H_2O under ultrasonication for 1 h. Then, 100 mg TiO_2/$MoSe_2$ composites (the amount of $MoSe_2$ is 0.1%) were added into the suspension. After constantly stirring for 2 h, the suspension was transferred into a 100 mL Teflon-sealed autoclave and kept at 120 °C for 3 h. After naturally cooling down, the sample was collected by centrifugation, rinsing with water and absolute ethanol, and drying at 60 °C for 12 h. The samples of 0.5%, 1.0%, 2.5%, and 5.0% mass ratios of γ-graphyne to TiO_2 were denoted as TiO_2/$MoSe_2$/0.5GY, TiO_2/$MoSe_2$/1.0GY, TiO_2/$MoSe_2$/2.5GY, and TiO_2/$MoSe_2$/5.0GY, respectively.

2.3 Characterizations

The samples were characterized by X-ray diffraction (Bruker D/8 advanced diffractometer with Cu Kα radiation), Raman spectra (HORIBA Jobin Yvon XploRA system with laser excitation wavelength of 532 nm), energy dispersive X-ray spectroscopy (EDS), transmission electron microscopy (TEM), and high-resolution TEM (Tecnai G2 F20 S-Twin FE-TEM). The X-ray photoelectron spectroscopy (XPS) was measured using an RBD upgraded PHI-5000 C ESCA system (Perkin Elmer) and analyzed by Augerscan software. The UV–Vis diffuse reflectance spectra (UV-3150 UV–Vis spectrophotometer) and photoluminescence (PL) spectra (F-4500, with an excitation wavelength of 330 nm) were recorded as well. The electrochemical impedance spectra (EIS) and Mott–Schottky plots were implemented on a PARSTAT 4000 Potentiostat/ Galvanostat EIS analyzer and corresponding test conditions were detailed in the Supporting Information.

2.4 Photocatalytic measurements

The photocatalytic hydrogen evolution was conducted in a photocatalytic system (Labsolar-IIIAG, Beijing Perfectlight Co., Ltd.). Typically, 20 mg photocatalysts were dispersed into 100 mL of 1:9 methanol/deionized water by sonication for 30 min. The obtained mixture was transferred into the reactor and then constantly stirred. Before irradiation, the reaction system was evacuated. A 300 W Xe arc lamp (PLS-SXE300, Beijing Perfectlight Co., Ltd.) with an optical filter was used to provide a simulated solar irradiation condition. The gas component was detected by an online gas chromatograph (Shiweipx, GC7806, TCD detector, Ar carrier and 5 Å molecular sieve columns). Three consecutive test cycles of the hydrogen evolution were carried out under identical experimental conditions.

3 Results and discussion

3.1 Characterizations of photocatalysts

The crystal structure and phase of the samples were characterized by XRD (Fig. 1a). Compared to bare TiO_2, the prominent diffraction peaks of TiO_2/$MoSe_2$, and TiO_2/$MoSe_2$/GY nanocomposites were almost the same, suggesting that the introduction of $MoSe_2$ and γ-graphyne has little effect on the crystallinity of TiO_2. No signals for $MoSe_2$ and γ-graphyne were found, probably owing to their relatively low amount and low diffraction intensity of 2D materials [42]. Raman spectra in Fig. 1b and 1c verify the presence of $MoSe_2$ and γ-graphyne in the TiO_2/$MoSe_2$/GY nanocomposite with the peak at 241 cm^{-1} to $MoSe_2$ nanosheets [34–50] and the typical D band at 1360 cm^{-1} and the G band at 1588 cm^{-1} to γ-graphyne [51, 52]. In the magnified Raman spectra (Fig. 1c), the peak intensity for both D band and G band raised gradually as the amount of γ-graphyne increased, further indicating that γ-graphyne was successfully loaded onto TiO_2/$MoSe_2$. XPS results also confirms the introduction of GY and $MoSe_2$ in the TiO_2-based nanocomposites (Fig. S1) [53, 54].

TEM images in Fig. 1d demonstrates that the layered γ-graphyne serves as a novel support that is uniformly decorated with TiO_2 and $MoSe_2$. The HRTEM pictures (Fig. 1e) display a typical lattice distance of 0.35 and 0.32 nm corresponding to the (101) plane of anatase TiO2 and (110) plane of rutile TiO_2, respectively. The obvious well-exfoliated nanosheets were found, with the distinct lattice spacing of 0.65 nm, which is in accordance with the (002) crystal plane of hexagonal $MoSe_2$. The (220) and (422) planes of the γ-graphyne were also observed. The EDS mapping images (Fig. 1f) revealed that the Ti, O, C, Mo, and Se were distributed in the selected area, which further indicates the formation of TiO_2/$MoSe_2$/GY multiple heterojunctions. Thus, a close neighborhood of TiO_2, $MoSe_2$, and γ-graphyne components was achieved by the hydrothermal processing, which is believed to favor the light absorption and the separation of photogenerated charge carriers in the ternary nanocomposites.

3.2 *Photocatalytic H_2 production activities*

The photocatalytic activities of the synthesized materials were evaluated for H_2 evolution from water splitting under simulated solar light irradiation, with methanol as hole scavenger. Our previous study shows that TiO_2/$MoSe_2$ nanocomposites with 0.1% of $MoSe_2$ possess the highest

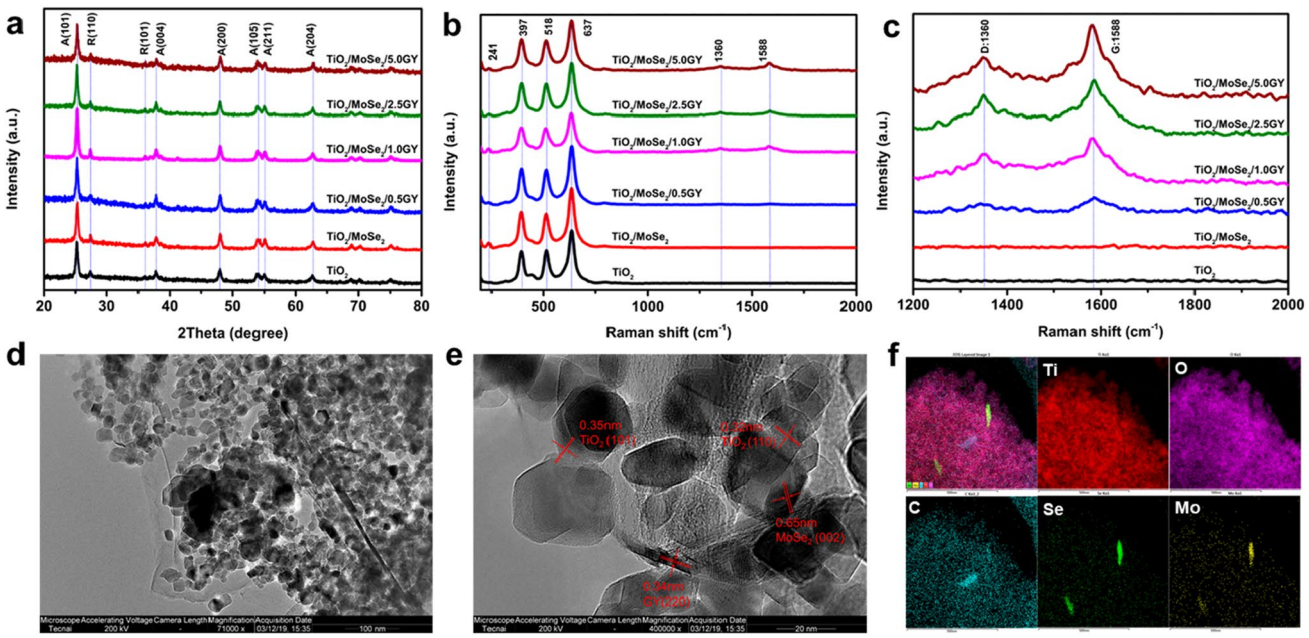

Fig. 1 **a** XRD patterns, **b** Raman spectra, **c** corresponding magnified Raman spectra, **d** TEM image, **e** HRTEM image, and **f** EDS mapping images of $TiO_2/MoSe_2$/GY nanocomposites. A: anatase phase; R: rutile phase

hydrogen generation rate [33]. In this work, optimized $MoSe_2$ amount with 0.1% is adopted for the design of ternary nanocomposites as shown in Fig. 2a. Figure 2b shows the photocatalytic H_2 evolution activities for the TiO_2 samples with 0.1% of $MoSe_2$ with different amounts of γ-graphyne from 0 to 5.0%. As the amounts of γ-graphyne increased, the hydrogen evolution of the nanocomposites raised. The optimized $TiO_2/MoSe_2$/2.5GY sample exhibited the highest H_2 production rate of 16 μmol h^{-1}, which was about 3.2-fold as high as that of $TiO_2/MoSe_2$, 1.4-fold as high as that of TiO_2/GY and 6.2-fold as high as that of TiO_2. The results were compared with the reported TiO_2 and $MoSe_2$-based nanocomposites for photocatalytic H_2 generation (Table 1). It can be seen that our ternary $TiO_2/MoSe_2$/GY nanocomposite has superior advantages. A further increase in the loading of γ-graphyne above the optimum level results in a decrease of the H_2 evolution rate, which is probably because excess γ-graphyne in the nanocomposites might prevent the exposure of TiO_2 to incident light and the generation of electrons from TiO_2, and possibly act as a recombination center for the photoexcited carriers [16].

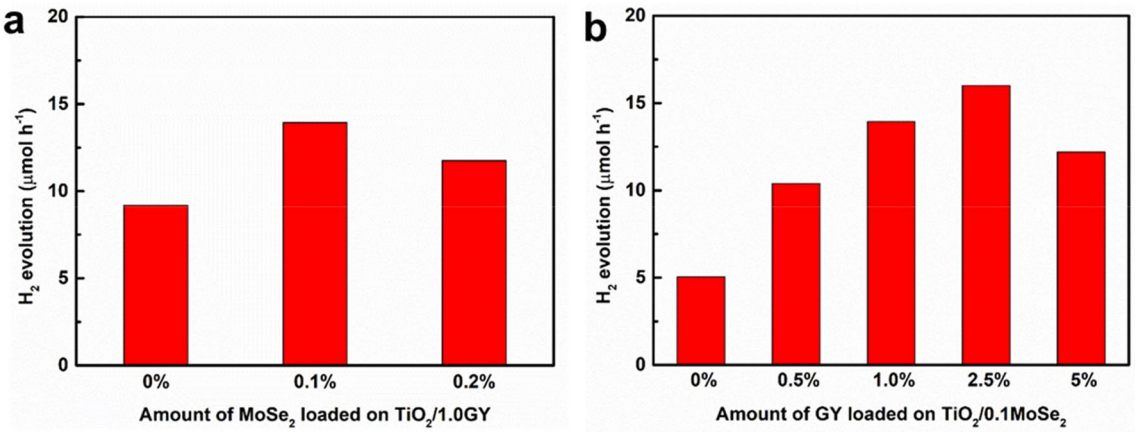

Fig. 2 **a** Hydrogen evolution rate of $TiO_2/MoSe_2$/GY nanocomposites with different amounts of $MoSe_2$, **b** hydrogen evolution rate of $TiO_2/MoSe_2$/GY nanocomposites with different amounts of γ-graphyne

Table 1 Comparison of the reported TiO_2 and $MoSe_2$-based composites for photocatalytic H_2 evolution

System	Sacrificial agent	Light source (wavelength/nm)	$v(H_2)$ (μmol h^{-1} g^{-1})	References
graphene/P25	25% methanol	350 W Xe lamp	456	[55]
rGO/P25	20% ethanol	200 W Xe lamp	740	[56]
TiO_2/MoS_2/graphene	25% ethanol	350 W Xe lamp	2000	[17]
p-MoS_2/n-rGO	50% ethanol	300 W Xe lamp	24.8	[57]
$MoSe_2$/g-C_3N_4	10% triethanolamine	300 W Xe lamp(> 420)	136.8	[58]
$TiO_2/MoSe_2$	10% methanol	300 W Xe lamp	252	[33]
TiO_2/γ-graphyne	10% methanol	300 W Xe lamp	555	[48]
$TiO_2/MoSe_2$/γ-graphyne	10% methanol	300 W Xe lamp	800	This work

Moreover, the stability of the photocatalysts were investigated. As shown in Fig. 3a, the $TiO_2/MoSe_2$/GY sample kept high hydrogen evolution activity around the three measurement cycles with good stability. The Raman spectra for $TiO_2/MoSe_2$/GY before and after the photocatalytic reaction is represented in Fig. 3b. The results demonstrate that no difference occurred for the Raman peaks ascribed to $MoSe_2$ and γ-graphyne, illustrating $MoSe_2$ and γ-graphyne should keep stable during the photocatalytic process. The results of cycling measurement along with Raman spectroscopy indicate the good stability of $TiO_2/MoSe_2$/GY photocatalysts.

3.3 Mechanism for the improved photocatalytic activity

The optical absorption property is the key factor to judge the photocatalytic activity of the samples. The optical performance of the samples was researched using UV–Vis diffuse reflectance spectra. As shown in Fig. 4a, the sample showed a red-shifted absorption edge with slightly enhanced absorption in the visible region after the loading of $MoSe_2$. Once the $MoSe_2$ and γ-graphyne were introduced together, the absorption edges of $TiO_2/MoSe_2$/GY samples exhibited a further red-shift (from 410 to 490 nm), indicating the improvement of the visible light absorption ability of the nanocomposite. Moreover, the color of the nanocomposites varied from white to gray, as revealed in the inserted pictures. The results suggest that the ternary nanocomposite may be able to absorb more light to produce electron–hole pairs and thus promise improved photocatalytic activities.

The electrochemical impedance spectroscopy (EIS) tests were performed to study the charge-transfer capacity (Fig. 4b). A suitable equivalent circuit model was proposed as shown in the inset in Fig. 4b. The data were fitted and are presented in Table S1. Therein, R_i is internal resistance, *CPE* is a constant phase element, R_{ct} is the charge transfer at the working electrode/electrolyte interface, respectively. The electrochemical impedance spectroscopy showed the smaller R_{ct} for $TiO_2/MoSe_2$/GY nanocomposites, demonstrating the efficient charge transfer by promoting the transportation of photo-induced carriers [59].

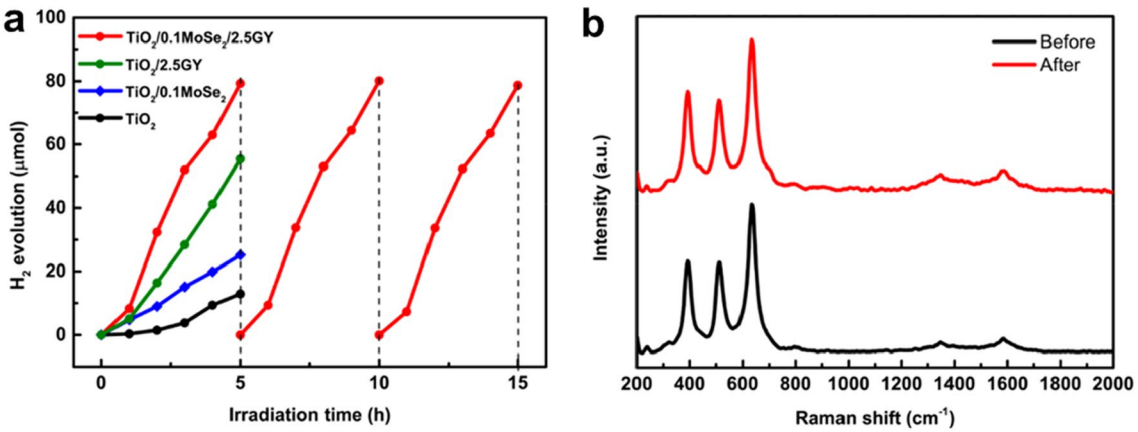

Fig. 3 **a** Cycling measurement of hydrogen evolution as a function of irradiation time and **b** Raman spectra of $TiO_2/MoSe_2$/2.5GY sample before and after photocatalytic reaction

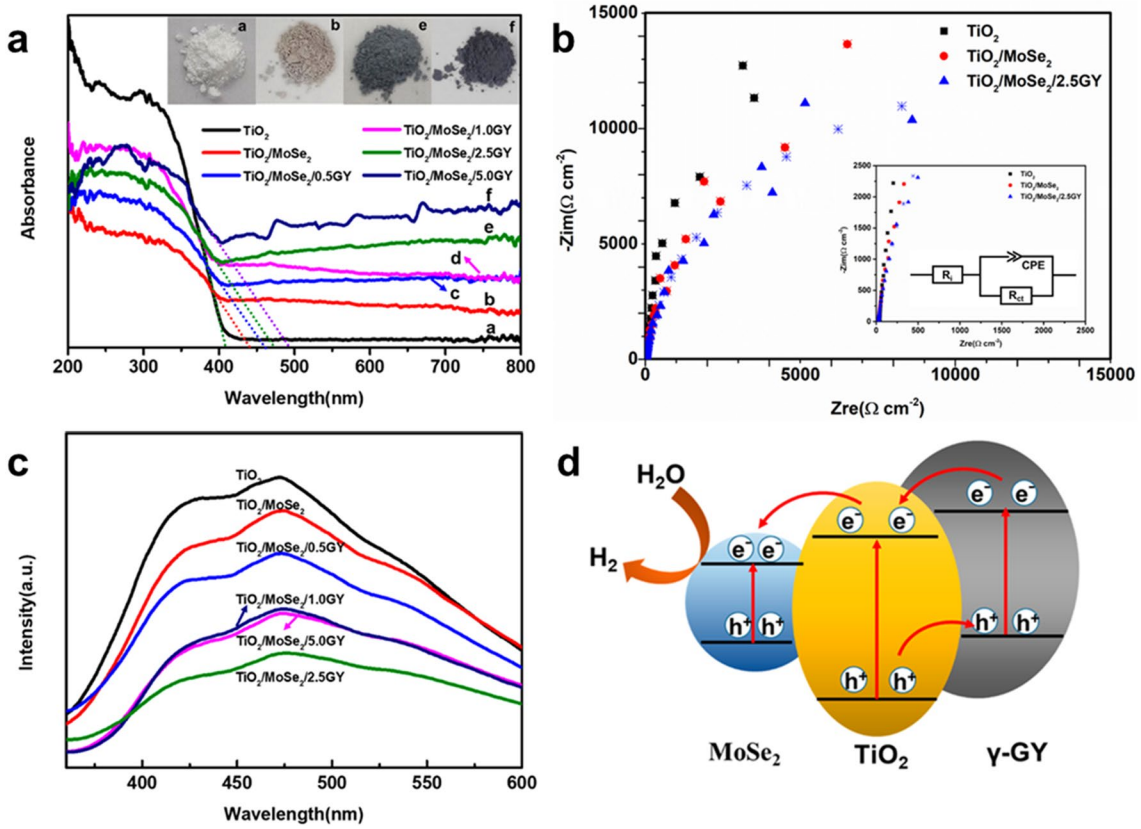

Fig. 4 **a** UV–Vis diffuse reflectance spectra, **b** electrochemical impedance spectroscopy (EIS), **c** photoluminescence (PL) spectra, and **d** possible mechanism for the $TiO_2/MoSe_2$/GY ternary nanocomposite

It is well known that the intensity of photoluminescence (PL) spectra is directly related to the recombination of charge carriers [60, 61]. Figure 4c reveals the PL spectra of TiO_2, $TiO_2/MoSe_2$, and $TiO_2/MoSe_2$/GY nanocomposites with the excitation wavelength of 330 nm, respectively. Pure TiO_2 showed the strongest intensity of PL emission peak, and it decreased when $MoSe_2$ was incorporated, indicating that the recombination of photogenerated charges was inhibited to some degree [60]. The PL intensity of $TiO_2/MoSe_2$/GY nanocomposites declined significantly as compared to $TiO_2/MoSe_2$ after the introduction of GY in the nanocomposites, indicating that γ-graphyne also played a leading role in reducing the recombination of photogenerated charges. The results show that the introduction of GY greatly accelerates the charge transfer and effectively suppress the recombination of photogenerated electron–holes, which explains its excellent photocatalytic water splitting activity for hydrogen evolution. Increased PL intensities were observed for $TiO_2/MoSe_2$/2.5GY with further increasing the amounts of GY, suggesting that a further increase of γ-graphyne led to relatively increased charge recombination.

As addressed by the UV–Vis DRS, EIS, and PL studies, the ternary nanocomposites afford the absorption of more light and fast charge-transfer capability with more charge carriers for the photocatalytic reaction, which improves the hydrogen generation performance. The bandgaps of $MoSe_2$ and γ-graphyne were characterized to be 1.80 and 2.7 eV, respectively (Fig. S2 and S3). The flat-band potentials (corresponding to the VB) for $MoSe_2$ and γ-graphyne were measured to be 2.27 and 2.19 V *vs.* NHE, respectively. A synergistic mechanism for the ternary nanocomposite is proposed as shown in Fig. 4d, based on the working functions of γ-graphyne (CB edge = -0.5 eV *vs.* NHE), TiO_2 (CB edge = -0.3 eV *vs.* NHE), and $MoSe_2$ (CB edge = 0.5 eV *vs.* NHE). Notably, in the present case of nanocomposite materials, a transfer of electrons from the CB of γ-graphyne into the CB of TiO_2, and from the TiO_2 CB to $MoSe_2$, has occurred due to the band matching. The VB of TiO_2 is more positive than the VB of γ-graphyne, providing a pathway for holes from the TiO_2 VB to γ-graphyne VB. It is assumed that this effective cascade-driven electronic mechanism [62] would isolate electron–hole pairs and decreases their recombination, thereby increasing the charge-transfer capability, which has been well demonstrated by PL analysis. Furthermore, the $MoSe_2$ nanosheets with active edge sites function as a

cost-effective cocatalyst, hence vastly facilitating the electrons separation and surface reactions.

4 Conclusion

In summary, we have demonstrated that $MoSe_2$ and γ-graphyne are effective agents to enhance the photocatalytic activities of TiO_2. The obtained ternary $TiO_2/MoSe_2$/GY exhibited cyclic stability and enhanced photocatalytic activities in H_2 evolution in contrast to those of the binary composites and individual components. A high photocatalytic hydrogen generation rate of 16 μmol h^{-1} was obtained, which was much higher than that of the $TiO_2/MoSe_2$ composites (5 μmol h^{-1}) and TiO_2 (2.58 μmol h^{-1}). The combined heterojunction enabling a cascade-driven electron transfer and synergistic effects of the nanocomposite account for the enhanced photocatalytic activity. Both $MoSe_2$ and γ-graphyne can improve the light absorption ability of the nanocomposites, which has been analyzed by UV–Vis DRS. Meanwhile, the $MoSe_2$ and γ-graphyne serve as an electron collector and a hole transfer channel, respectively, which can separate the photogenerated electron–hole pairs effectively and suppress their recombination, and thus favor enhanced photocatalytic activity. The $MoSe_2$ nanosheets on the surface of TiO_2 would promote the surface shuttling properties for efficient H_2 production due to their high active edge sites and superior electrical conductivity. This work suggests that the construction of ternary photocatalysts is an effective approach toward the rising demand for solving energy and environmental problems.

Acknowledgements The authors gratefully acknowledge the financial support of the National Natural Science Foundation of China (No. 21273047).

Compliance with ethical standards

Conflicts of interest There are no conflicts to declare.

References

1. S. Wang, P. Chen, Y. Bai, J. Yun, G. Liu, L. Wang, New BiVO4 dual photoanodes with enriched oxygen vacancies for efficient solar-driven water splitting. Adv Mater **30**, 1800486 (2018)
2. D.M. Schultz, T.P. Yoon, Solar synthesis: prospects in visible light photocatalysis. Science **343**, 1239176 (2018)
3. D. Jun, J. Xia, H. Li, Z. Liu, Freestanding atomically-thin two-dimensional materials beyond graphene meeting photocatalysis: opportunities and challenges. Nano Energy **35**, 79–91 (2017)
4. X. Zhang, H. Li, X. Cui, Y. Lin, Graphene/TiO2 nanocomposites: synthesis, characterization and application in hydrogen evolution from water photocatalytic splitting. J Mater Chem A **20**, 2801–2806 (2010)
5. X. Li, J. Shi, H. Hao, X. Lang, Visible light-induced selective oxidation of alcohols with air by dye-sensitized TiO2 photocatalysis. Appl Catal B-Environ **232**, 260–267 (2018)
6. Y. Ma, X. Wang, Y. Jia, X. Chen, H. Han, C. Li, Titanium dioxide-based nanomaterials for photocatalytic fuel generations. Chem Rev **114**, 9987–10043 (2014)
7. S. Thangavel, K. Krishnamoorthy, V. Krishnaswamy, N. Raju, J. Sang, G. Venugopal, Graphdiyne-ZnO nanohybrids as an advanced photocatalytic material. J Phys Chem C **119**, 22057–22065 (2015)
8. J. Lv, Z. Zhang, J. Wang, X. Lu, W. Zhang, T. Lu, In situ synthesis of CdS/Graphdiyne heterojunction for enhanced photocatalytic activity of hydrogen production. Appl Mater Interfaces **11**, 2655–2661 (2019)
9. H. Xie, Y. Zhao, H. Li, Y. Xu, X. Chen, 2D BiVO4/g-C3N4 Z-scheme photocatalyst for enhanced overall water splitting. J Mater Sci **54**(15), 10836–10845 (2019)
10. X. Chen, S. Mao, Titanium dioxide nanomaterials: synthesis, properties, modifications, and applications. Chem Rev **107**, 2891–2959 (2007)
11. S. Hoang, S. Guo, N. Hahn, A. Bard, C. Mullins, Visible light driven photoelectrochemical water oxidation on nitrogen-modified TiO2 nanowires. Nano Lett **12**, 26–32 (2012)
12. Y. Yuan, Z. Ye, H. Lu, B. Hu, Y. Li, D. Chen, J. Zhong, Z. Yu, Z. Zou, Constructing anatase TiO2 nanosheets with exposed (001) facets/layered MoS2 two dimensional nanojunction for enhanced solar hydrogen generation. ACS Catal **6**, 532–541 (2016)
13. S. Meng, J. Zhang, S. Chen, S. Zhang, W. Huang, Perspective on construction of heterojunction photocatalysts and the complete utilization of photogenerated charge carriers. Appl Surf Sci **476**, 982–992 (2019)
14. J. Low, J. Yu, M. Jaroniec, S. Wageh, A. Al-Ghamdi, Heterojunction photocatalysts. Adv Mater **29**, 1601694 (2017)
15. H. Wang, L. Zhang, Z. Chen, J. Hu, S. Li, Z. Wang, J. Liu, X. Wang, Semiconductor heterojunction photocatalysts: design, construction, and photocatalytic performances. Chem Soc Rev **43**, 5234–5244 (2014)
16. B. Sun, W. Zhou, H. Li, L. Ren, P. Qiao, W. Li, H. Fu, Synthesis of particulate hierarchical tandem heterojunctions toward optimized photocatalytic hydrogen production. Adv Mater **30**, 1804282 (2018)
17. Q. Xiang, J. Yu, M. Jaroniec, Synergetic effect of MoS2 and graphene as cocatalysts for enhanced photocatalytic H2 production activities of TiO2 nanoparticles. J. Am Chem Soc **134**, 6575–6578 (2012)
18. M. Wu, L. Li, Y. Xue, G. Xu, L. Tang, N. Liu, W. Huang, Fabrication of ternary GO/g-C3N4/MoS2 flower-like heterojunctions with enhanced photocatalytic activities for water remediation. Appl Catal B-Environ **228**, 103–112 (2018)
19. J. Shen, J. Wu, L. Pei, M. Rodrigues, Z. Zhang, F. Zhang, X. Zhang, P. Ajayan, M. Ye, CoNi2S4-graphene-2D-MoSe2 as an advanced electrode material for supercapacitors. Adv Energy Mate **6**, 1600341 (2016)
20. H. Tian, M. Liu, W. Zheng, Constructing 2D graphitic carbon nitride nanosheets/layered MoS2/graphene ternary nanojunction with enhanced photocatalytic activities. Appl Catal B **225**, 468–476 (2018)
21. X. Wang, Y. Gong, G. Shi, W. Chow, K. Keyshar, G. Ye, R. Vajtai, J. Lou, Z. Liu, E. Ringe, B. Tay, P. Ajayan, Chemical vapor deposition growth of crystalline mono layer MoSe2. ACS Nano **8**, 5125–5131 (2014)
22. K. Kim, J. Lee, D. Nam, H. Cheong, Davydov splitting and excitonic resonance effects in Raman spectra of few-layer MoSe2. ACS Nano **10**, 8113–8120 (2016)

23. Z. Hu, Z. Wu, C. Han, J. He, Z. Ni, W. Chen, Two-dimensional transition metal dichalcogenides: interface and defect engineering. Chem Soc Rev **47**, 3100–3128 (2018)
24. U. Gupta, C. Rao, Hydrogen generation by water splitting using MoS2 and other transition metal dichalcogenides. Nano Energy **41**, 49–65 (2017)
25. B. Liu, X. Liu, L. Li, Z. Zhuge, Y. Li, C. Li, Y. Gong, L. Niu, S. Xu, C.Q. Sun, CaIn2S4 decorated WS2 hybrid for efficient Cr (VI) reduction. Appl Surf Sci **484**, 300–306 (2019)
26. H. Chu, W. Lei, X. Liu, J. Li, W. Zheng, G. Zhu, C. Li, L. Pan, C. Sun, Synergetic effect of TiO2 as co-catalyst for enhanced visible light photocatalytic reduction of Cr(VI) on MoSe2. Appl Catal A **521**, 19–25 (2016)
27. S. Mao, Z. Wen, S. Ci, X. Guo, K. Ostrikov, J. Chen, Perpendicularly oriented MoSe2/graphene nanosheets as advanced electrocatalysts for hydrogen evolution. Small **11**, 414–419 (2016)
28. Y. Wang, J. Zhao, Z. Chen, F. Zhang, W. Guo, H. Lin, F. Qu, Construction of Z-scheme MoSe2/CdSe hollow nanostructure with enhanced full spectrum photocatalytic activities. Appl Catal B **244**, 76–86 (2019)
29. D. Kong, H. Wang, J. Cha, M. Pasta, K. Koski, J. Yao, Y. Cui, Synthesis of MoS2 and MoSe2 films with vertically aligned layers. Nano Lett **13**, 1341–1347 (2013)
30. Z. Ren, X. Liu, Z. Zhuge, Y. Gong, C.Q. Sun, MoSe2/ZnO/ZnSe hybrids for efficient Cr (VI) reduction under visible light irradiation. Chinese J Catal **41**, 180–187 (2020)
31. C. Tsai, K. Chan, F. Pedersen, J. Norskov, Active edge sites in MoSe2 and WSe2 catalysts for the hydrogen evolution reaction: a density functional study. Phys Chem Chem Phys **16**, 13156–13164 (2014)
32. T. Xie, Y. Liu, H. Wang, Z. Wu, Layered MoSe2/Bi2WO6 composite with p-n heterojunctions as a promising visible-light induced photocatalyst. Appl Surf Sci **444**, 320–329 (2018)
33. L. Wu, S. Shi, Q. Li, X. Zhang, X. Cui, TiO2 nanoparticles modified with 2D MoSe2 for enhanced photocatalytic activities on hydrogen evolution. Int J Hydrog Energy **44**, 720–728 (2019)
34. G. Wang, S. Zhang, X. Zhang, L. Zhang, Y. Cheng, D. Fox, H. Zhang, J. Coleman, W. Blau, J. Wang, Tunable nonlinear refractive index of two-dimensional MoS2, WS2, and MoSe2 nanosheet dispersions. Photonics Res **3**, A51–A55 (2015)
35. S. Chen, T. Takata, K. Domen, Particulate photocatalysts for overall water splitting. Nat Rev Mater **2**, 17050 (2017)
36. Y. Li, L. Xu, H. Liu, Y. Li, Graphdiyne and graphyne: from theoretical predictions to practical construction. Chem Soc Rev **43**, 2572–2586 (2014)
37. A. Puigdollers, G. Alonso, P. Gamallo, First-principles study of structural, elastic and electronic properties of α-, β- and γ-graphyne. Carbon **96**, 879–887 (2016)
38. K. Srinivasu, S. Ghosh, Graphyne and graphdiyne: promising materials for nanoelectronics and energy storage applications. J Phys Chem C **116**, 5951–5956 (2012)
39. G. Li, Y. Li, H. Liu, Y. Guo, Y. Lia, D. Zhu, Architecture of graphdiyne nanoscale films. Chem Commun **46**, 3256–3258 (2010)
40. Z. Jia, Y. Li, Z. Zuo, H. Liu, C. Huang, Y. Li, Synthesis and properties of 2D carbon-graphdiyne. Acc Chem Res **50**, 2470–2478 (2017)
41. C. Huang, Y. Li, N. Wang, Y. Xue, Z. Zuo, H. Liu, Y. Li, Progress in research into 2D graphdiyne-based materials. Chem Rev **118**, 7744–7803 (2018)
42. S. Wang, L. Yi, J. Halpert, X. Lai, Y. Liu, H. Cao, R. Yu, D. Wang, Y. Li, A novel and highly efficient photocatalyst based on P25-graphdiyne nanocomposite. Small **8**, 265–271 (2012)
43. J. Li, X. Gao, B. Liu, Q. Feng, X. Li, M. Huang, Z. Liu, J. Zhang, C. Tung, L. Wu, Graphdiyne: a metal-free material as hole transfer layer to fabricate quantum dot sensitized photocathodes for hydrogen production. J Am Chem Soc **138**, 3954–3957 (2016)
44. Y. Han, X. Lu, S. Tang, X. Yin, Z. Wei, T. Lu, Metal-free 2D/2D heterojunction of graphitic carbon nitride/graphdiyne for improving the hole mobility of graphitic carbon nitride. Adv Energy Mater **8**, 1702992 (2018)
45. X. Kong, Y. Huang, Q. Liu, Two-dimensional boron-doped graphyne nanosheet: a new metal-free catalyst for oxygen evolution reaction. Carbon **123**, 558–564 (2017)
46. Q. Li, Y. Li, Y. Chen, L. Wu, C. Yang, X. Cui, Synthesis of γ-graphyne by mechanochemistry and its electronic structure. Carbon **136**, 248–254 (2018)
47. Q. Li, C. Yang, L. Wu, H. Wang, X. Cui, Converting benzene into γ-graphyne and its enhanced electrochemical oxygen evolution performance. J. Mater Chem A **7**, 5981–5990 (2019)
48. L. Wu, Q. Li, C. Yang, X. Ma, Z. Zhang, X. Cui, Constructing a novel TiO2/γ-graphyne heterojunction for enhanced photocatalytic hydrogen evolution. J Mater Chem A **6**, 20947–20955 (2018)
49. C. Yang, Y. Li, Y. Chen, Q. Li, L. Wu, X. Cui, Mechanochemical synthesis of γ-graphyne with enhanced lithium storage performance. Small **15**, 1804710 (2019)
50. S. Li, H. Miyazaki, H. Song, H. Kuramochi, S. Nakaharai, K. Tsukagoshi, Quantitative Raman spectrum and reliable thickness identification for atomic layers on insulating substrates. ACS Nano **6**, 7381–7388 (2012)
51. S. Zhang, J. Wang, Z. Li, R. Zhao, L. Tong, Z. Liu, J. Zhang, Z. Liu, Raman spectra and corresponding strain effects in graphyne and graphdiyne. J Phys Chem C **120**, 10605–10613 (2016)
52. R. Liu, X. Gao, J. Zhou, H. Xu, Z. Li, S. Zhang, Z. Xie, J. Zhang, Z. Liu, Chemical vapor deposition growth of linked carbon monolayers with acetylenic scaffoldings on silver foil. Adv Mater **29**, 1604665 (2017)
53. B. Sun, W. Zhou, H. Li, L. Ren, P. Qiao, F. Xiao, L. Wang, B. Jiang, H. Fu, Magnetic Fe2O3/mesoporous black TiO2 hollow sphere heterojunctions with wide-spectrum response and magnetic separation. Appl Catal B **221**, 235–242 (2018)
54. W. Zhou, W. Li, J. Wang, Y. Qu, Y. Yang, Y. Xie, K. Zhang, L. Wang, H. Fu, D. Zhao, Ordered mesoporous black TiO2 as highly efficient hydrogen evolution photocatalyst. J Am Chem Soc **136**, 9280–9283 (2014)
55. Q. Xiang, J. Yu, M. Jaroniec, Enhanced photocatalytic H2-production activity of graphene-modified titania nanosheets. Nanoscale **3**, 3670–3678 (2011)
56. W. Fan, Q. Lai, Q. Zhang, Y. Wang, Nanocomposites of TiO2 and reduced graphene oxide as efficient photocatalysts for hydrogen evolution. J Phys Chem C **115**, 10694–10701 (2011)
57. K. Meng, J. Li, S. Cushing, M. Zhi, N. Wu, Solar hydrogen generation by nanoscale p-n junction of p-type molybdenum disulfide/n-type nitrogen-doped reduced graphene oxide. J Am Chem Soc **135**, 10286–10289 (2013)
58. D. Zeng, P. Wu, W. Ong, B. Tang, M. Wu, H. Zheng, Y. Chen, D. Peng, Construction of network-like and flower-like 2H-MoSe2 nanostructures coupled with porous g-C3N4 for noble-metal-free photocatalytic H2 evolution under visible light. Appl Catal B **233**, 26–34 (2018)
59. B. Luo, R. Song, J. Geng, X. Liu, D. Jing, M. Wang, C. Cheng, Towards the prominent cocatalytic effect of ultra-small CoP particles anchored on g-C3N4 nanosheets for visible light driven photocatalytic H2 production. Appl Catal B **256**, 117819 (2019)
60. Y. Zhang, W. Zhu, X. Cui, W. Yao, T. Duan, One-step hydrothermal synthesis of Bi-TiO2 nanotube/graphene composites: an efficient photocatalyst for spectacular degradation of organic pollutants under visible light irradiation. Appl Catal B **218**, 758–769 (2017)
61. C. Yang, Z. Wang, T. Lin, H. Yin, X. Lv, D. Wan, T. Xu, C. Zheng, J. Lin, F. Huang, X. Xie, M. Jiang, Core-shell nanostructured "black" rutile titania as excellent catalyst for hydrogen production

enhanced by sulfur doping. J Am Chem Soc **135**, 17831–17838 (2013)
62. S. Obregón, Y. Zhang, G. Colón, Cascade charge separation mechanism by ternary heterostructured BiPO4/TiO2/g-C3N4 photocatalyst. Appl Catal B **184**, 96–103 (2016)